CrossMark

Low-Cycle Fatigue Testing Using a Small Specimen of Sn-58Bi Solder at 313 K and 353 K

FUMIO OGAWA [iD],[1,4] NORITAKE HIYOSHI,[2] YUTAKA KONISHI,[3] and TAKAMOTO ITOH[1]

1.—Department of Mechanical Engineering, College of Science and Engineering, Ritsumeikan University, 1-1-1, Nojihigashi, Kusatsu, Shiga 525-8577, Japan. 2.—Department of Mechanical Engineering, University of Fukui, 3-9-1 Bunkyo, Fukui-shi, Fukui 910-8507, Japan. 3.—Graduate School of Science and Engineering, Ritsumeikan University, 1-1-1, Nojihigashi, Kusatsu, Shiga 525-8577, Japan. 4.—e-mail: ogawa-f@fc.ritsumei.ac.jp

Low-cycle fatigue tests using small specimens of Sn-58Bi solder have been performed at 313 K and 353 K. The samples had a gage diameter and gage length of 3 mm and 6 mm, respectively. The tests were conducted in strain-control mode, using triangular waveforms with a strain rate of 0.5%/s over a total strain range of 0.5% to 1.5%. The failure life was longer at 353 K than at 313 K, and the slope of the total strain range against failure life at 353 K was steeper than at 313 K. Stress amplitude was retained at 313 K even beyond the middle of the sample fatigue life, but decreased dramatically just before failure due to the brittleness of the specimen. However, at 353 K, the number of cycles to failure was greater after the initial decrease in stress amplitude because of the increase in crack resistance (ductility) of the specimen when hot. The morphology of cracks was affected by the temperature of the test. The main crack that appeared at 313 K was smooth and oriented nearly perpendicular to the specimen axial direction. However, the crack that formed at 353 K had a zigzag shape. The increased ductility and crack resistance at 353 K contributed to the increased failure life at higher temperatures.

Key words: Lead-free solder, low-cycle fatigue, Sn-58Bi solder, thermal effects, crack morphology

INTRODUCTION

Solder alloys are widely used to connect electrical components. Currently, use of lead solders is restricted by Restriction of Hazardous Substances (RoHS) directives, and lead-free solders have become standard.[1–3] However, the fatigue and mechanical properties of lead-free solders are not fully understood. During use of electrical equipment, the temperature of each component varies as the device is switched on and off. Stresses arise in the solder that holds onboard components together, because of the different thermal expansion coefficients of electrical components.[4] This cyclic loading can cause low-cycle fatigue damage to solder. Therefore, strength testing of lead-free solders under fatigue loading is essential to prevent failure during the operating life of electronic devices.[5–7] Generally, the mechanical properties of lead-free solders change significantly with the size of the solder. However, standard-sized bulk specimens are typically used in fatigue testing of lead-free solders. These fatigue tests can be expensive because of the large amounts of material used in the processing of the samples.[8,9] In a previous study, a fatigue testing technique using a small specimen of solders with gage diameter of 3 mm was reported, and the fatigue strength of Sn-3.0Ag-0.5Cu and Sn-5Sb solders at 313 K reported.[10] The fatigue strength obtained using small specimens coincides well with that obtained using standard-sized bulk specimens,

Table I. Chemical composition of Sn-58Bi solder (wt.%)

	Sn	Ag	Cu	Sb	Bi	Pb	Zn	Fe	Al	As
Sn-58Bi	42.1	< 0.001	0.006	< 0.001	Bal.	0.01	< 0.001	< 0.001	< 0.001	0.003

confirming the validity of such fatigue testing using small specimens.

Here, this low-cycle fatigue testing approach was applied to Sn-58Bi solder, Sn-58Bi solders have low melting point and were developed for use in step-soldering processes.[11–14] They are favorable for soldering of temperature-sensitive components and substrates. Additionally, Sn-58Bi solders have higher mechanical strength and creep resistance and lower ductility than lead solders.[15,16] To the best of the authors' knowledge, the fatigue properties of Sn-58Bi solder have not been widely studied. In particular, reports on the fatigue properties of small specimens of Sn-58Bi solders are sparse. Sn-58Bi solder was tested at 313 K and 353 K to examine how temperature affects its fatigue performance. The crack propagation characteristics under fatigue loading and the effects on the fatigue strength at different temperatures are also discussed.

EXPERIMENTAL PROCEDURES

Table I presents the chemical composition of the solder tested in this study.

Sn-58Bi is a eutectic solder consisting of Sn and Bi, and its microstructure has been studied.[17]

Figure 1 shows the shape and dimensions of the small fatigue specimen, with total length, gage length, and diameter at the gage of 55 mm, 6 mm, and 3 mm, respectively. Details of the preparation of the specimen have been reported previously.[10]

A horizontal electrical servohydraulic push–pull machine was employed for fatigue testing. The specimen was heated using an electric furnace. A thermocouple was set at an R portion (Fig. 1) to prevent cracks from starting at the gage section. To keep the temperature in the gage section at the target temperature (313 K or 353 K), the temperature in the gage section was measured using a thermocouple, and the difference in temperature between the gage section and R portion recorded. The temperature in the gage section was controlled within ±1 K of the target temperature. An extensometer was attached to the gage section using dots of epoxy resin. To prevent the specimen from buckling due to the bending force applied during installation of the extensometer, a balancing force was applied in the opposite direction utilizing coil springs and heat-resistant string (Fig. 2).

Strain-controlled low-cycle fatigue tests were performed at 313 K and 353 K. The total strains applied were 0.5%, 0.7%, 1.0%, and 1.5%. Triangular waveforms with 0.5%/s strain rate were used to
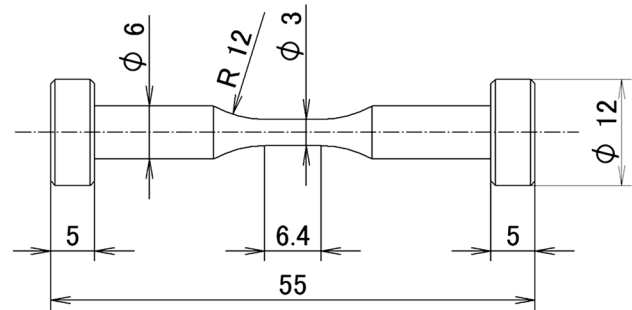

Fig. 1. Shape and dimensions of the specimen (mm).

apply the strain. The number of cycles to failure (failure life) N_f was defined as the number of cycles after which the specimen broke or showed a 25% drop in tensile stress amplitude from that at the middle of the fatigue life of the specimen.[18]

RESULTS AND DISCUSSION

Figure 3 shows the correlation of the failure life with the total strain range at 313 K and 353 K, with the values of the slope shown on each curve. The failure life at 353 K was longer than that at 313 K. Additionally, the slope of the lifecycle curve at 353 K was slightly greater than that at 313 K.

Figure 4 shows the correlation of the failure life with the plastic strain range at 313 K and 353 K, with the values of the slope on each curve. The slope of the curve at 313 K is 0.26, while that at 353 K is 0.32. The slope is steeper at 353 K because the specimen experiences lower peak stress during the loading cycles. The failure life can be expressed using the Coffin–Manson equation,[19–21] adopting the plastic strain range $\Delta\varepsilon_p$:

$$\Delta\varepsilon_p \times N_f^\beta = C, \tag{1}$$

where β and C are 0.26 and 9.53 at 313 K, or 0.32 and 20.0 at 353 K, respectively.

Figure 5a and b show hysteresis loops under the strain range of 1.0% at 313 K and 353 K, respectively. Closed symbols mark data taken at the beginning of the test, gray symbols mark data taken at the middle of the fatigue life, and open symbols mark data recorded just before failure.

The hysteresis loops show that the stress did not decrease during the first half of the specimen's failure life. However, the stress decreased sharply at the end of the test. Stress relaxation and softening were more apparent in the specimen tested at 353 K than at 313 K. These effects increase the failure life for large plastic strain

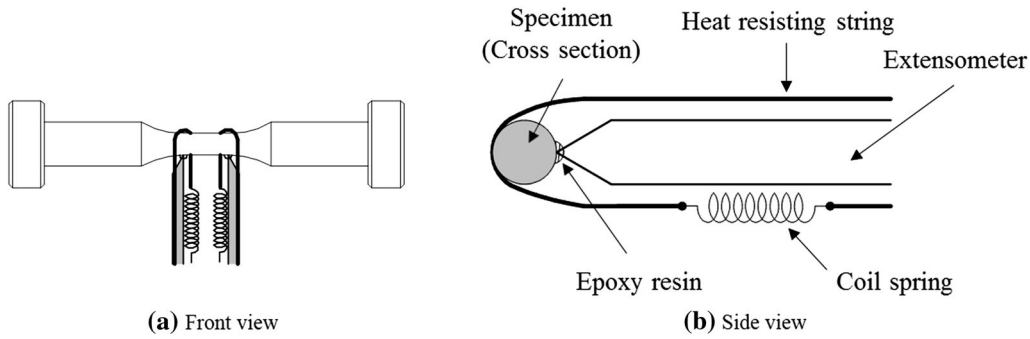**(a)** Front view　　　　　**(b)** Side view

Fig. 2. Method for attachment of the extensometer to the specimen: (a) front and (b) side view.
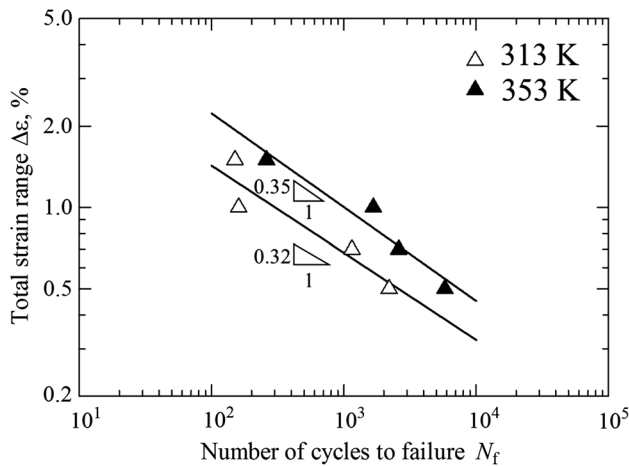

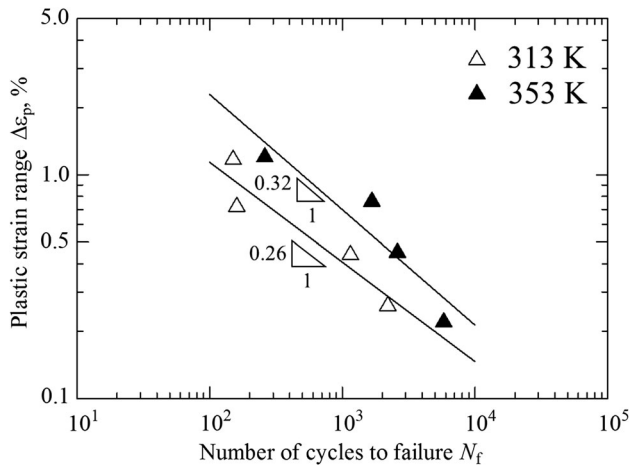Fig. 3. Correlation between number of cycles to failure and total strain range.

Fig. 4. Correlation of number of cycles to failure with plastic strain range.

Fig. 5. Hysteresis loops at (a) 313 K and (b) 353 K.

ranges and steepen the slope of the life curve at 353 K (Fig. 4). Figure 5b shows the decrease in the Young's modulus, yield stress, and cyclic hardening rate, leading to an increase in ductility at 353 K.
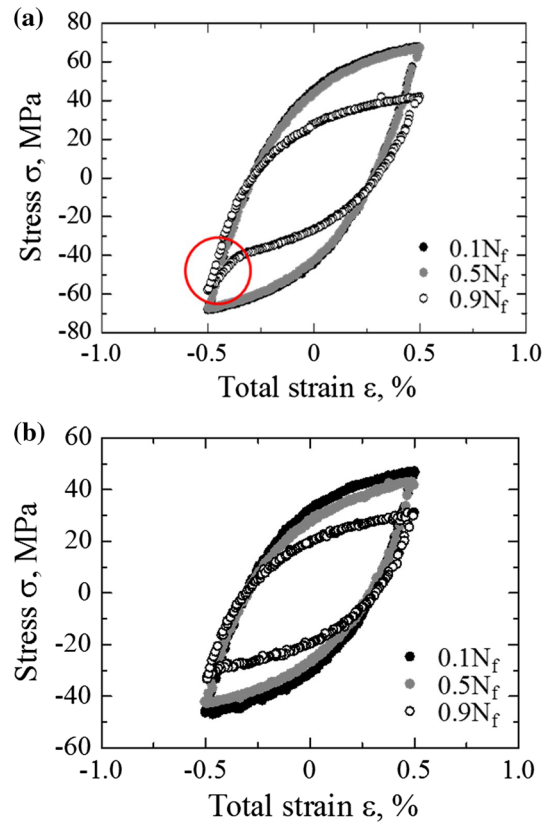
The coarsening of the solder microstructure explains these effects. However, this decrease in the mechanical properties of the specimen causes no change in the plastic strain range at different temperatures. The curvature in the hysteresis loop at $0.9N_f$ cycles in Fig. 5a is attributed to crack closure and is indicated using a red circle.

Figure 6 compares the hysteresis loops at $0.5N_f$ at a total strain range of 1.5%. The decrease in the cyclic hardening rate and peak stress is confirmed at 353 K. This decrease in stress contributes to the longer fatigue life of the specimen at 353 K.

Figure 7a and b show the variation in the stress amplitude with the number of cycles at 313 K and
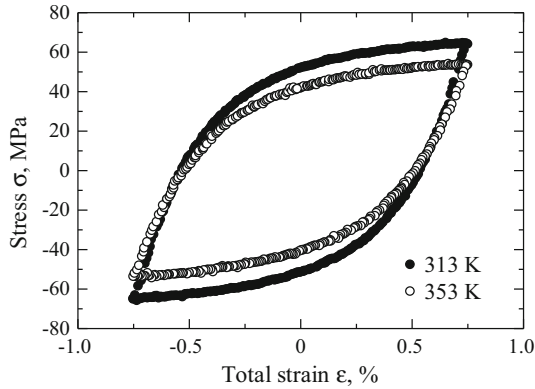
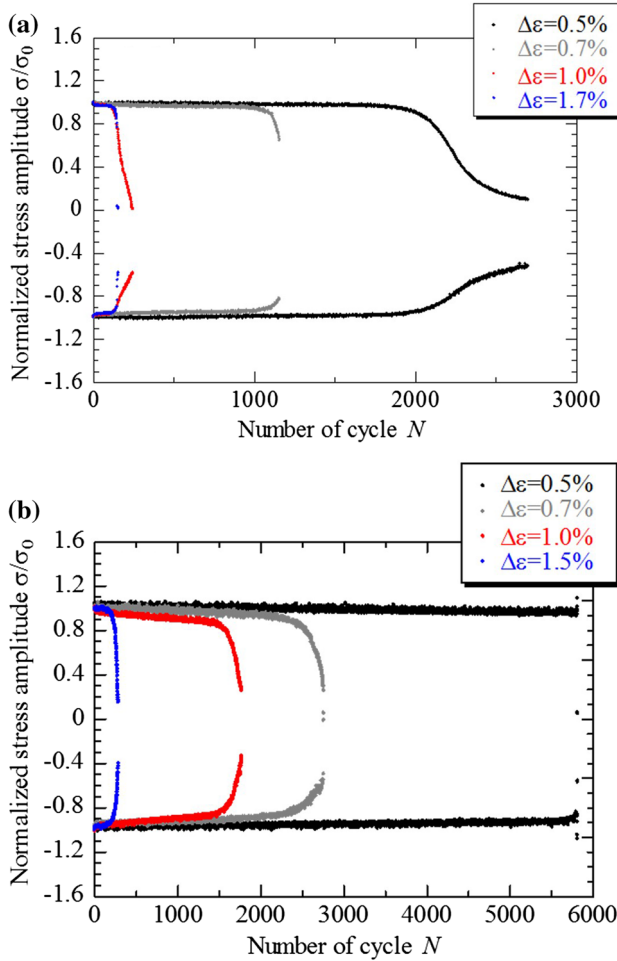Fig. 6. Comparison of hysteresis loops at 313 K and 353 K.

Fig. 7. Variation of stress amplitude of Sn-58Bi with number of cycles at (a) 313 K and (b) 353 K.

353 K, respectively. In this figure, the stress amplitudes are normalized to the initial measurements. Some stress amplitude was retained at 313 K even after the middle of the fatigue test, then gradually decreased, likely indicating that the main crack grew due to the coalescence of microcracks in the

specimen. Higher total strain ranges caused a sudden decrease in the normalized stress range immediately after the initiation of the fatigue test, due to a faster crack propagation rate. The increased ductility and crack resistance at 353 K explain the longer fatigue life of this specimen after the initiation of the decrease in the stress amplitude.

Figure 8 shows macroscopic photos of the fatigued specimen. Failure occurred within the gage section for each, but cracks began where the extensometer was attached under the following conditions: total strain range of 0.7% at 313 K, and total strain range of 0.5% and 1.0% at 353 K. For the total strain range of 0.7% at 353 K, the crack began outside the gage section, but the specimen did not bend or buckle, which demonstrates that the fatigue tests were successful. Comparison of the test results at 313 K and 353 K (Fig. 8) reveals that the fractured surface at 313 K was perpendicular to the specimen's axis, while the fractured surface at 353 K was inclined at 45° from the specimen axis. This indicates that the fractured surface changed from brittle to shear because of the increase in temperature.

The fatigue cracks were also imaged in detail to elucidate the fatigue failure mechanism. Figure 9 shows an enlarged view of the cracks. The propagation of the main crack likely caused failure of the specimen, although ripples appeared at 353 K, probably caused by slippage. These ripples are marked using white arrows and indicate that the fatigued specimen retained some ductility. This ductility delayed the fatigue fracture at 353 K. The main crack that formed at 313 K was smooth and oriented almost perpendicular to the specimen's axial direction, while that formed at 353 K had a zigzag shape. The increased ductility at 353 K explains this difference in the cracking behavior and confirms that the longer failure life at 353 K can be attributed to the improved crack resistance.

Chen et al.[22] investigated the deformation behavior of Sn-58Bi solder alloys under tensile loading at 298 K and 348 K and found that softening and an improvement of ductility occur at 348 K. The deformation mechanism changes from dislocation glide to climb, which then improves the ductility of the specimen at higher temperatures. This mechanism qualitatively explains the longer failure life and the zigzag shape of the main crack at 353 K.

Figure 10a shows a magnification of the main crack at the total strain range of 0.7% and 313 K, while Fig. 10b displays a magnification of the main crack at the total strain range of 0.7% and 353 K.

Comparison of Fig. 10a and b clarifies that the grains coarsened when fatigued at 353 K. The microcracks can be observed, as indicated by black arrows in the figure. Yoon et al.[17] investigated

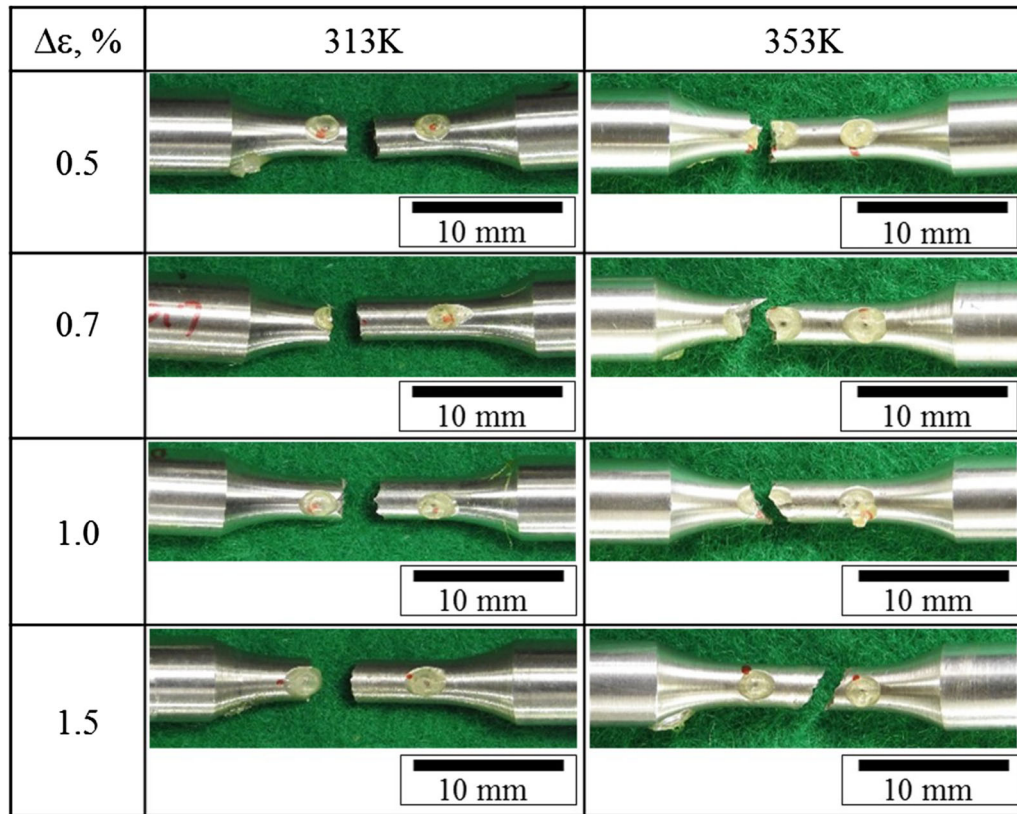| Δε, %	313K	353K
0.5	10 mm	10 mm
0.7	10 mm	10 mm
1.0	10 mm	10 mm
1.5	10 mm	10 mm

Fig. 8. Photo of the specimen after failure.

isothermal aging of Sn-58Bi solder and found extensive coarsening of the Bi-rich and Sn-rich phases during aging, which is consistent with the behavior shown in Fig. 10. This coarsening may promote the propagation of microcracks inside the grains and grain boundaries. However, the decrease in peak stress and increase in fracture toughness increase the fatigue life at 353 K. Therefore, both transgranular and intergranular fractures likely occurred.

Figure 11 shows images of the fractured surfaces taken using scanning electron microscopy. The origins of fatigue cracks are indicated by green arrows. Figure 11a shows that the fractured surface is flat for the total strain range of 0.7% at 313 K, and that the crack propagated soon after the initiation. Figure 11b shows that, for the total strain range of 0.7% at 353 K, cracks began at the surface of the specimen. However, a crack also began inside the specimen, indicated with a white circle. As evident from the rough fractured surface, ductility governed the fatigue fracture at 353 K. Figure 11c shows that, for the total strain range of 1.5% at 313 K, the fractured surface was flat and the microstructure of the solder was fine.

Figure 11d shows that, for the total strain range of 1.5% at 353 K, around the green arrows, a small amount of beach marks appears. Dislocation clearly drove the fatigue fracture in this case. Nevertheless, almost no change occurred in the plastic strain range at different temperatures, although the fatigue life was longer at higher temperatures. The fracture mode changed from rapid propagation of cracks starting at the specimen surface to ductility-controlled fatigue fracture at higher temperatures.

The specimens endured more cycles before failure at 353 K than at 313 K. Sn-58Bi solder is brittle at room temperature and is therefore sensitive to the strain rate, but the specimen became more ductile at higher temperatures. The results obtained in this study will be useful for a range of applications of Sn-58Bi solder.

CONCLUSIONS

1. Low-cycle fatigue tests of Sn-58Bi solder using a small specimen were successfully performed, and fatigue properties that can be
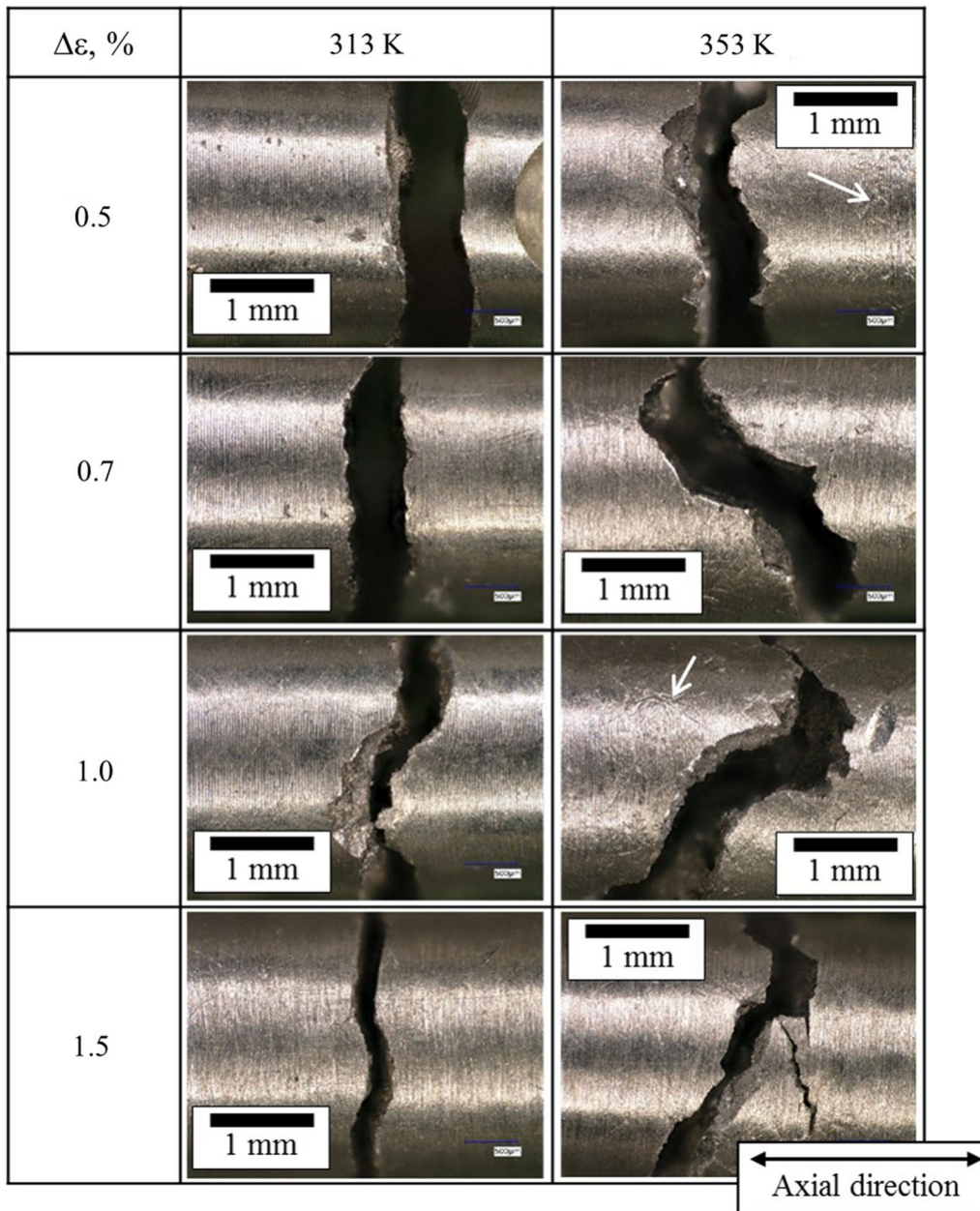
Fig. 9. Crack observation results.

used in the design of solders for practical use were measured.

2. The specimen lasted longer at 353 K than at 313 K. Stress amplitude was retained even after the middle of the life of the sample at 313 K, while it decreased dramatically around the end of its life due to the brittleness of the specimen. Conversely, at 353 K,

more cycles passed before failure after the specimen started to crack. The specimen was more resistant to cracking at higher temperatures.

3. The main crack at 313 K was smooth and oriented almost perpendicular to the specimen's axial direction. On the other hand, the main crack that formed at 353 K had a zigzag
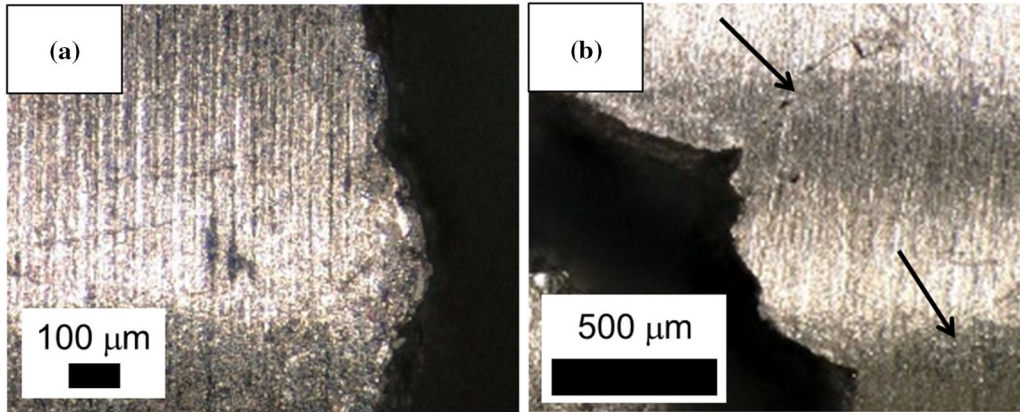
Fig. 10. Magnification of main cracks at (a) total strain range of 0.7% at 313 K and (b) total strain range of 0.7% at 353 K.
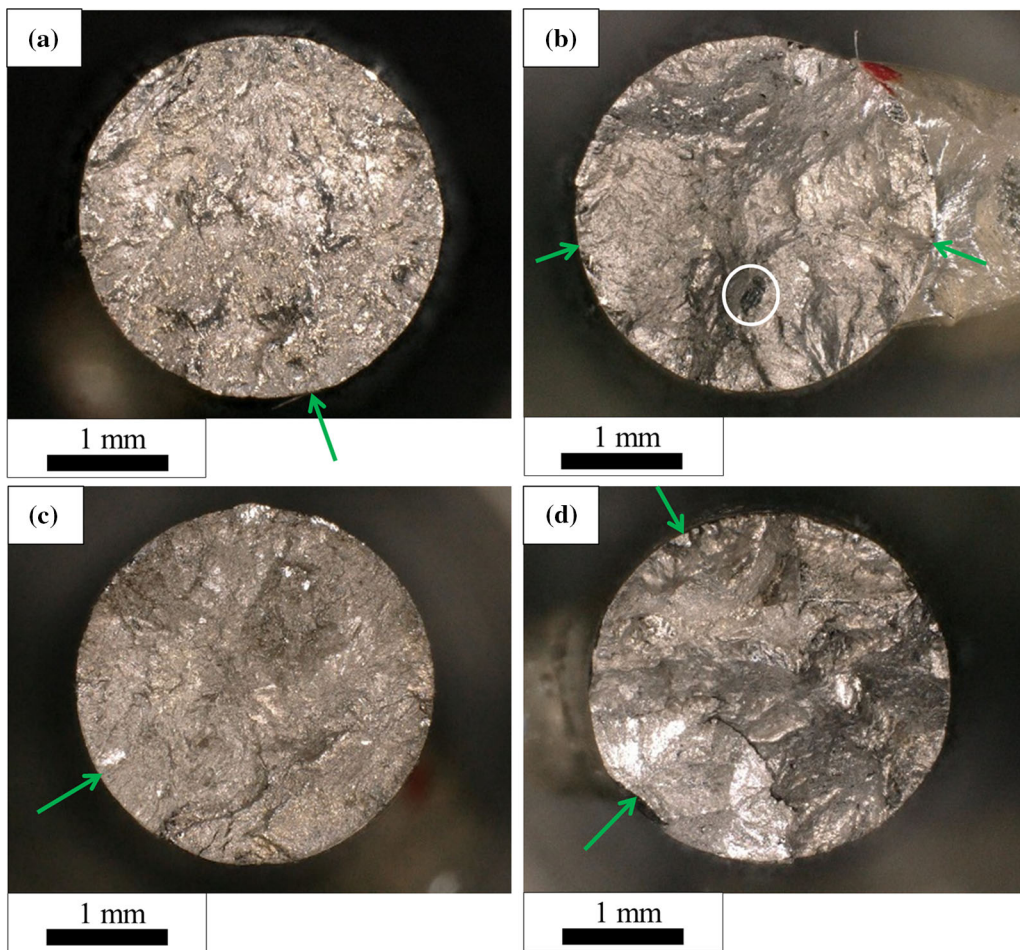

Fig. 11. Observation results of fractured surface for (a) total strain range of 0.7% at 313 K, (b) total strain range of 0.7% at 353 K, (c) total strain range of 1.5% at 313 K, and (d) total strain range of 1.5% at 353 K.

shape. The increased ductility and crack resistance at 353 K contributed to the longer failure life at this temperature. Observations of the fractured surface support the above explanation.

REFERENCES

1. J. Glazer, *J. Electron. Mater.* 23, 693 (1994).
2. K.J. Puttlitz and K.A. Stalter, *Handbook of Lead-Free Solder Technology for Microelectronic Assemblies* (Boca Raton: CRC Press, 2004), pp. 1–48.
3. S. Cheng, C.M. Huang, and M. Pecht, *Microelectron. Reliab.* 75, 77 (2017).

4. Y. Tsukada, H. Nishimura, M. Sakane, and M. Ohnami, *J. Electron. Packag.* 122, 207 (2000).
5. A. Takada, M. Sakane, and Y. Tsukada, *J. Soc. Mater. Sci. Jpn.* 56, 129 (2007).
6. K. Suganuma, *Introduction to Lead-Free Soldering* (Osaka: Osaka University Press, 2013).
7. Z. Mei, J.W. Morris, M.C. Shine, and T.S.E. Summers, *J. Electron. Mater.* 20, 599 (1991).
8. M. Nozaki, M. Sakane, Y. Tsukada, and H. Nishimura, *J. Eng. Mater. Technol.* 128, 142 (2006).
9. F. Ogawa, T. Itoh, and T. Yamamoto, *Int. J. Fatigue* 110, 215 (2018).
10. Y. Konishi, T. Itoh, M. Sakane, F. Ogawa, and H. Kanayama, *Key Eng. Mater.* 734, 194 (2017).
11. Z. Mei and J.W. Morris, *J. Electron. Mater.* 21, 6 (1992).
12. F. Yang, L. Zhang, Z.Q. Liu, S.J. Zhong, J. Ma, and L. Bao, *Adv. Mater. Sci. Eng.* 2016 (2016).
13. F. Wang, Y. Huang, Z. Zhang, and C. Yan, *Materials (Basel)* 10, 8 (2017).
14. R.K. Shiue, L.W. Tsay, C.L. Lin, and J.L. Ou, *J. Mater. Sci.* 38, 6 (2003).
15. L.E. Felton, C.H. Raeder, and D.B. Knorr, *JOM* 45, 28 (1993).
16. C.H. Raeder, L.E. Felton, V.A. Tanzi, and D.B. Knorr, *J. Electron. Mater.* 23, 611 (1994).
17. J.W. Yoon, C.B. Lee, and S.B. Jung, *Mater. Trans.* 43, 1821 (2002).
18. H. Kanayama, Y. Konishi, F. Ogawa, T. Itoh, M. Sakane, M. Yamashita, and H. Hokazono, *Int. J. Fatigue* 116, 180 (2018).
19. C. Kanchanomai, Y. Miyashita, and Y. Mutoh, *J. Electron. Mater.* 31, 456 (2002).
20. S. Chen, P. Sun, X.C. Wei, Z.N. Cheng, and J. Liu, *Solder Surf. Mt. Technol.* 21, 48 (2009).
21. J.H. Kuang, C.M. Hsu, and A.D. Lin, *Integr. Ferroelectr.* 172, 200 (2016).
22. X. Chen, J. Zhou, F. Xue, and Y. Yao, *Mater. Sci. Eng. A* 662, 251 (2016).